Journal of Alloys and Compounds 895 (2022) 162689

Contents lists available at ScienceDirect

Journal of Alloys and Compounds

journal homepage: www.elsevier.com/locate/jalcom

The grain-refinement mechanism during heavy cold-rolling of commercial-purity titanium

S. Mironov[a,*], S. Zherebtsov[a], S.L. Semiatin[b]

[a] Belgorod National Research University, Pobeda 85, Belgorod 308015, Russia
[b] Air Force Research Laboratory, Materials and Manufacturing Directorate (ret'd), Wright-Patterson AFB, OH 45433-7817, USA

ARTICLE INFO

Article history:
Received 21 September 2021
Received in revised form 3 November 2021
Accepted 5 November 2021
Available online 12 November 2021

Keywords:
Commercial-purity titanium
Cold rolling
Ultrafine-grain materials
Electron backscatter diffraction (EBSD)
Microstructure

ABSTRACT

Microstructure evolution in heavily-cold-rolled (≥40 pct.) commercial-purity titanium was determined to be governed by a continuous-dynamic-recrystallization mechanism. This process was shown to be closely linked with mechanical twinning occurring at lower rolling strains. Specifically, twinning provided a nearly-twofold increase in flow stress due to pronounced work hardening. Twinning also led to the activation of additional (non-prism-<a>) slip modes, and thus markedly enhanced the progressive development of dislocation boundaries. As a result, a bulk ultrafine-grain structure was produced at relatively-low strains achievable by conventional flat rolling.

1. Introduction

It is often believed that the production of ultrafine-grain (UFG) materials requires specially-designed severe-plastic-deformation (SPD) techniques [1–3]. For commercial-purity titanium (CP Ti), on the other hand, it has been shown recently that a UFG structure can be developed during conventional cold rolling [4–8]. Such observations have thus spurred renewed interest in the underlying microstructural behavior of this material.

From a broad perspective, research over the last two decades has revealed a very specific pattern of microstructure evolution during cold rolling of CP Ti. In particular, it has been well established that at low-to-moderate strains (≤40–50 pct. rolling reduction) the refinement mechanism is governed by extensive mechanical (deformation) twinning. At larger strains, however, slip-induced microstructural changes become dominant [4,9–13].

Among the various twinning modes available in CP Ti, compression $\{11\bar{2}2\}$ and tensile $\{10\bar{1}2\}$ twin systems are typically reported [4–6,9,10,12–19]. In some cases, a small fraction of tensile $\{11\bar{2}1\}$ twins has also been noted [14,19,20]. The activated twinning system in most cases occurs in grains with preferential crystallographic orientations which satisfy a critical-resolved-shear-stress (Schmid) criterion [9,18–20]. Sometimes, there have been reports of $\{11\bar{2}1\}$ twins which deviate from Schmid's Law, presumably due to complex states of stress generated by local grain-to-grain interactions [19,21]. An essential characteristic of the twinning process is the typical activation of multiple twin families within each grain [7,9,10,14,15,19,20]. Specifically, secondary $\{10\bar{1}2\}$ twins are often observed within primary $\{1\bar{1}22\}$ twins [10,14,15,20]. In addition to the secondary twins, several variants of a given twinning mode are also frequently found within the same grain [14].

In addition to crystallographic orientation, the activation of twinning is also influenced greatly by the grain size [6,10,22]. For instance, extensive twinning is only observed for grain sizes larger than ~15 μm in CP Ti, whereas almost no twinning has been observed for grains with a size smaller than ~1 μm [6]. In particular, the $\{10\bar{1}2\}$ twinning mode has been reported to be particularly sensitive to the grain size [22]. Moreover, twinning provides a marked reduction in grain size, thereby being a very effective mechanism of grain refinement. However, because of the sensitivity of twinning to the crystallographic orientation of parent grains, it typically results in an inhomogeneous microstructure in which twinned areas are drastically refined while regions deformed by slip remain coarse-grained [9,15,20]. In addition, the inhibition of twinning in grains with a size below ~1 μm also tends to prevent the formation of a uniform UFG structure.

Another important feature of twins concerns the evolution of their misorientations relative to the associated matrix with continued straining. Not surprisingly, such misorientations experience a gradual transformation into ordinary (non-twin-related) grain

* Corresponding author.
E-mail address: mironov@bsu.edu.ru (S. Mironov).

https://doi.org/10.1016/j.jallcom.2021.162689
0925-8388/

boundaries [e.g. 23, 24], via a phenomenon usually attributed to diverging rotations of the adjoining twin and matrix due to a difference in slip activity.

For cold-rolling strains above ~50 pct., twinning is gradually suppressed due to progressive grain refinement. At this stage of deformation, the original twins are almost completely transformed into irregularly-shaped grains integral with the remainder of the microstructure. From a broad perspective, increased straining results in substantial increases in the misorientations of low-angle boundaries (LABs) [e.g. 23] and the eventual formation of high-angle boundaries (HABs) with a spacing of ~0.5 μm [7,23] that delimit the grains of a bulk UFG structure. Despite this refinement, such a UFG microstructure often retains a measurable portion (up to 15 pct.) of coarse-grained remnants whose crystallographic orientations are usually close to the stable orientation associated with rolling [7]. It is important to note that the microstructure of heavily-rolled CP Ti is also usually characterized by a very high dislocation density and that no clear dislocation-cell structure is typically found [4,5,7,9].

Recently, a strain-induced martensitic transformation has been reported to occur in heavily-rolled titanium [25–27]. This effect has been attributed to the splitting of perfect dislocations into two partials which should result in a new face-centered-cubic phase [25]. However, subsequent thorough examinations of this phenomenon have shown that the new phase was likely titanium hydride (TiH) which has been mistakenly identified as strain-induced martensite [28,29].

While twinning at relatively-low rolling strains has been well characterized, the details of microstructure evolution in *heavily-rolled* material are still poorly understood. The objective of the present study was to provide insight for this regime of deformation using the advanced capabilities of the electron back scatter diffraction (EBSD) technique.

2. Material and experimental procedures

The material used in the present investigation was CP Ti grade VT1–0 (per its Russian designation) with a nominal chemical composition shown in Table 1. It was received as a hot-rolled plate of 4-mm thickness, which had a fully-recrystallized structure with a mean grain size of 15 μm.

Samples measuring $30 \times 20 \times 4\ mm^3$ were machined from the plate and then flat rolled at ambient temperature and a constant rolling speed of 30 mm/s. To investigate microstructure evolution during rolling, various samples were rolled to different total thickness reductions, viz., 5, 10, 15, 30, 40, 60, or 90 pct., which corresponded to true thickness strains of 0.05, 0.10, 0.16, 0.22, 0.36, 0.51, 0.92, and 2.66, respectively. The relatively large gap in material conditions between true strains of 0.92 and 2.66 was chosen because of the apparent saturation of microstructural changes over this range, as has been found in the authors' previous work [23]. For each total reduction, unidirectional, multi-pass rolling was applied with a reduction per pass of ~5 pct. Although deformation heating was not quantified precisely, freshly-rolled sheets were only slightly warm to the touch and thus the rolling temperature surely remained much below 100 °C (≈$0.19T_m$, where T_m is the titanium melting point). The typical flat-rolling convention was adopted with the rolling, transverse, and thickness/normal directions being denoted as RD, TD, and ND, respectively.

Following cold rolling, microstructure observations were focused on the mid-thickness portion of the rolled sheets, and were conducted on the rolling plane (containing the RD and TD) using optical and transmission electron microscopy (TEM) in addition to extensive EBSD characterization. For the optical observations, specimens were mechanically polished using standard metallographic techniques and then etched in a solution of HF, HNO_3 and H_2O at a ratio of 1:2:3. A suitable surface finish for EBSD was obtained by applying mechanical polishing in a similar fashion followed by final electropolishing in a solution of 80-pct. acetic anhydride +20-pct. perchloric acid (chilled to ~10 °C) at an applied potential of 60 V. TEM specimens were prepared using electrical-discharge machining (EDM), grinding on each side to a thickness of ~0.1 mm, and then jet-polishing in a solution containing 5-pct. perchloric acid, 35-pct. butanol, and 60-pct. methanol at −30 °C.

Table 1
Nominal chemical composition of program material (wt. pct.).

Ti	Fe	Si	O	C	N	H
Balance	≤0.2	≤0.10	≤0.20	≤0.07	≤0.04	≤0.01

EBSD was conducted in an FEI Quanta 600 field-emission-gun scanning-electron microscope (FEG SEM) equipped with a TSL OIM™. The SEM was operated at an accelerating voltage of 30 kV. Depending on the particular material condition, the EBSD scan step size was varied from 2 μm (in the initial material) to 0.05 μm (90-pct. rolled material). Due to the relatively-high dislocation density in heavily-rolled specimens, which degraded the Kikuchi patterns somewhat, a relatively-slow EBSD acquisition rate was utilized to obtain reliable data. To improve the fidelity of EBSD results, grains comprising three or fewer pixels were automatically removed ("cleaned") from EBSD maps using the standard grain-dilation option of the TSL software. Due to the limited angular accuracy of EBSD, misorientations below 2° were excluded from consideration. A 15° criterion was applied to differentiate low-angle boundaries (LABs) from high-angle boundaries (HABs). The grain size was measured using the circle-equivalent-diameter approach [30].

TEM observations were performed with a JEOL JEM-2100FX transmission electron microscope operated at 200 kV.

To provide additional insight into microstructural changes during rolling, Vickers microhardness measurements and tensile tests were also performed. Tension specimens were machined parallel to the RD and had a gauge section measuring 16-mm length (RD) and 3-mm width (TD). The specimens were pulled to failure at ambient temperature and a nominal strain rate of $10^{-3}\ s^{-1}$ using an Instron 5882 universal testing machine.

3. Results

3.1. Wok hardening during rolling

Tensile behavior and microhardness measurements as a function of rolling strain (Fig. 1) provided indirect insight into the broad aspects of microstructure evolution.

As expected, cold rolling gave rise to a significant increase in strength but a large reduction in ductility, the latter quantified by the relatively-low uniform elongation (strain at maximum load/engineering stress) exhibited in engineering stress-strain curves (Fig. 1a). Characterized by either the yield stress or the microhardness, the strength of CP-Ti nearly doubled after 90-pct. reduction (rolling strain ≈2.7) (Fig. 1b, c). For both metrics, the strength increased noticeably to a true strain of ~1.0, but then tended to saturate. This trend is common for severely-deformed metallic materials and is usually attributed to a dynamic balance between the hardening and recovery processes.

Estimates of the hardening rate $dX/d\varepsilon$, in which X denotes the yield strength or microhardness increase as a function of true strain ε, provided additional insight into the strengthening effect of cold rolling (Fig. 1d, e). The peak hardening rate was observed at a true strain of ~0.1–0.2, i.e., at a very early stage in rolling. In CP Ti (as well as in other hexagonal metals), this behavior is often attributed to twinning at low strains.

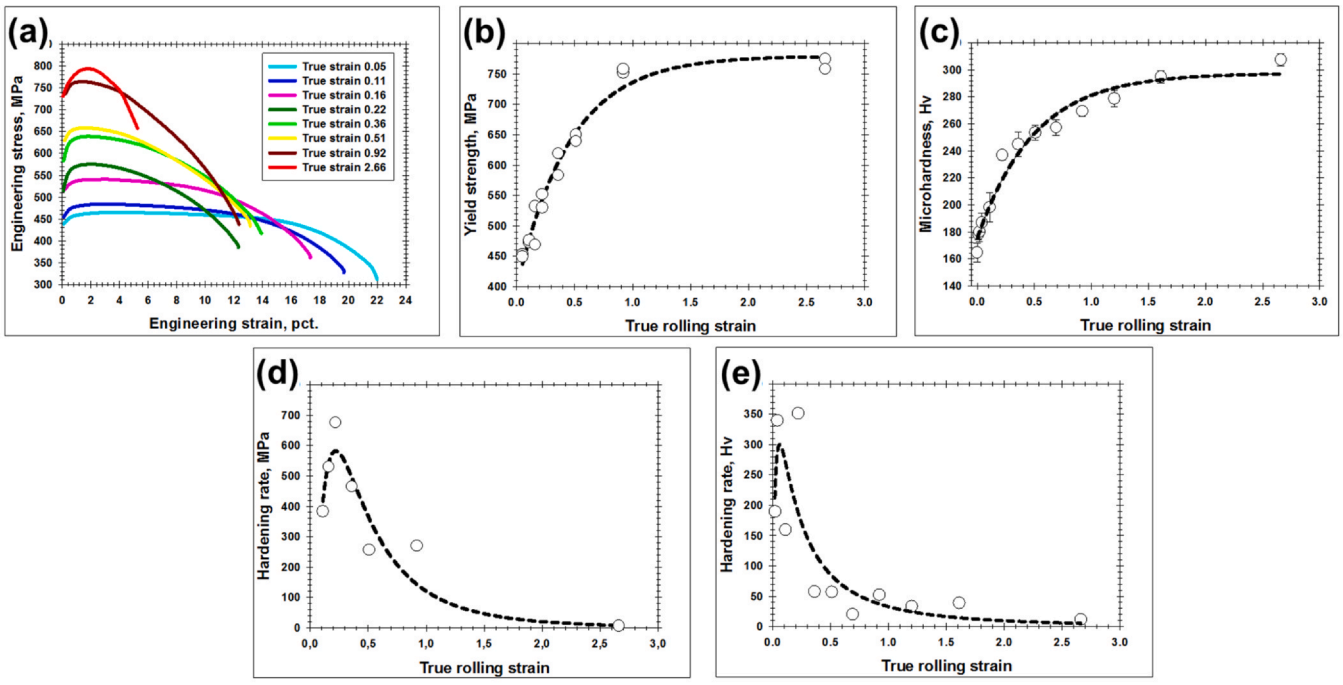

Fig. 1. Effect of rolling strain on mechanical behavior: (a) Engineering stress-strain curves, (b) yield strength, (c) mean microhardness, (d) strain-hardening rate derived from yield-strength measurements, and (e) strain-hardening rate derived from microhardness measurements.

3.2. Optical microstructure observations

Optical (rolling-plane) micrographs taken after various imposed strains (Fig. 2) confirmed that the initial stage of microstructure evolution was characterized by abundant twinning (Fig. 2a and b). The twins had diverse morphologies, including lenticular, wedge, and rectangular ones, and varied in both longitudinal and transverse dimensions. In many cases, parallel twins tended to lie in a group and occupy a significant portion of a deformed grain. Intersecting sets of twins were also observed within the same grain. Furthermore, secondary twins were also often found within relatively-coarse twins. Despite these features, some grains remained untwinned or contained only occasional twins. These latter occurrences are usually explained in terms of the crystallographic orientation of such grains being favorable for prism-<a> slip with its low critical resolved shear stress (CRSS) [7,9,15].

At true strains of 0.36 and above, the original grains exhibited an elongation along the rolling direction (Fig. 2c to e), presumably due to the geometric requirements of the imposed strain. On the other hand, the twin boundaries tended to lose their original morphology and gradually transform into irregular-shaped microstructural elements (Fig. 2e). The relatively-dark appearance of former twins in etched specimens suggested a relatively-high dislocation density (Fig. 2c to e).

At the highest rolling reductions, the contours of the original grains were barely recognizable (Fig. 2f), presumably due to

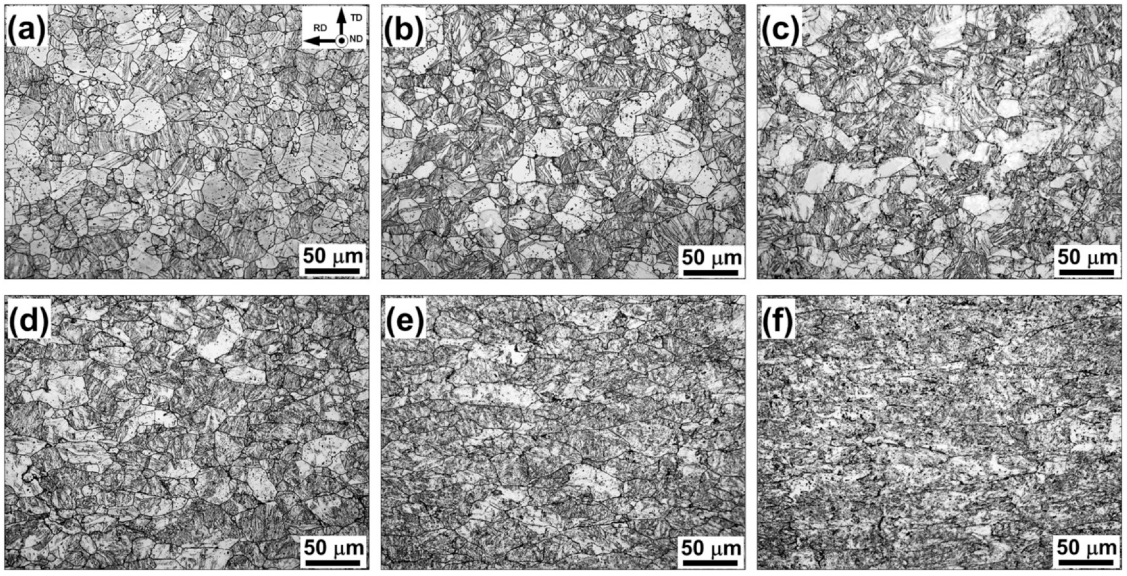

Fig. 2. Optical micrographs showing microstructures developed for true rolling strains of: (a) 0.05, (b) 0.22, (c) 0.36, (d) 0.51, (e) 0.92, or (f) 2.66.

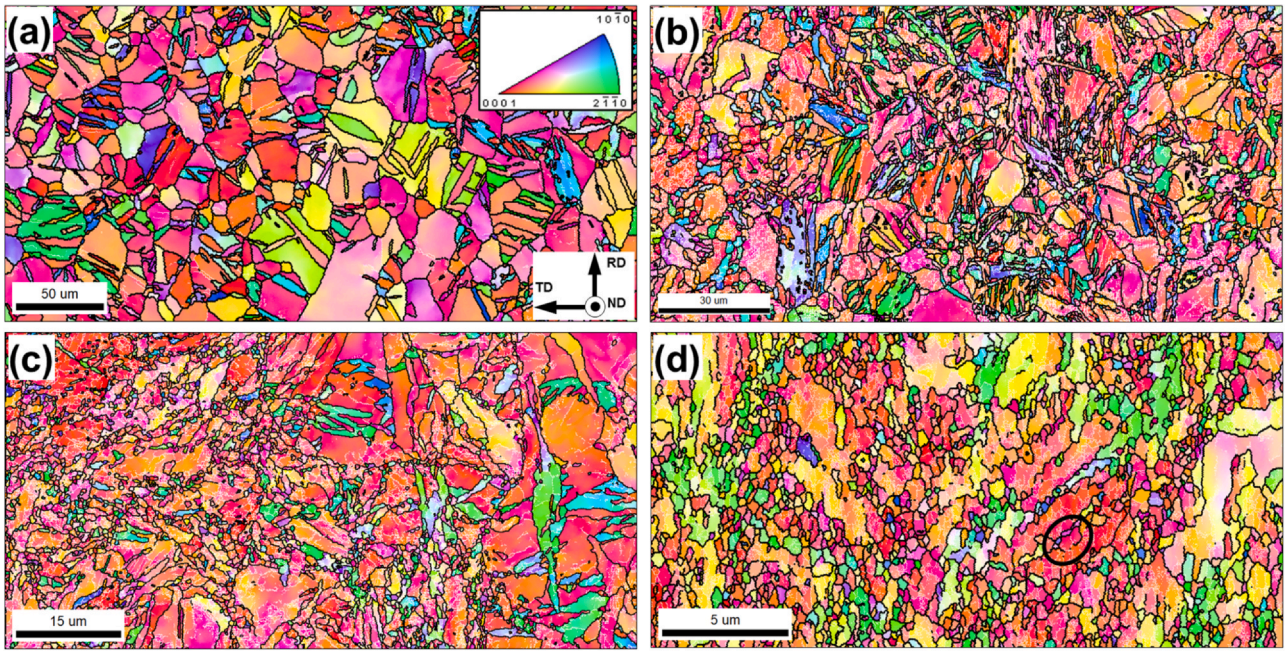

Fig. 3. Selected portions of normal-direction EBSD inverse-pole-figure maps showing microstructure developed during cold rolling to a true strain of: (a) 0.11, (b) 0.36, (c) 0.92, or (d) 2.66. In the maps, LABs and HABs are depicted as white or black lines, respectively. In (d), the circled area illustrates the gradual transformation of subgrains to grains.

extensive development of internal substructure. Nevertheless, a significant portion of the parent-grain remnants had still survived (Fig. 2f).

3.3. EBSD results: microstructure morphology and grain size

EBSD inverse-pole-figure (ipf) maps from rolled specimens (Fig. 3) and related data derived from the ipf maps (Figs. 4–9) provided deeper insight into the details of microstructure evolution. The EBSD measurements confirmed extensive mechanical twinning at low rolling strains (Fig. 3a). This process promoted a shift in the grain-size distribution toward smaller grains (Fig. 4a) and reduced the mean grain size (Fig. 4b). However, the refinement in microstructure was not uniform, and a noticeable fraction of grains contained almost no twins (Fig. 3a). An increase in strain noticeably enhanced the formation of LABs (Fig. 3b and c). In contrast to the behavior for cubic metals [e.g. 31], the dislocation boundaries were not arranged into a lamellar-type microstructure, but were distributed irregularly within grains. The ultrafine grains had developed by a strain of 0.92 (Fig. 3b to c and 4a). Accordingly, the overall *mean* grain size achieved was ~1 μm by this level of deformation (Fig. 4b). However, grain-refinement was noted to still be fairly heterogeneous (Fig. 3c), and the resulting microstructure could not be categorized as a uniform fine-grain one. At the strain of 0.92, it was also clearly seen that twins which had nucleated at much lower strains tended to lose their original morphology and were thus transformed into irregular-shaped grains (Fig. 3c).

After rolling to the highest imposed strain ($\varepsilon = 2.66$), the fraction of ultrafine-grains had increased significantly thus giving rise to a distinctly-bimodal microstructure (Figs. 3d, 4a). In addition, the ultrafine-grains tended to be clustered preferentially near original grain boundaries and/or within former twins, thereby giving rise to a necklace-type microstructure. From the specific character of microstructure morphology (highlighted, for instance, by the circled area in Fig. 3d), it seems that the ultrafine-grains originated from a gradual transformation of LABs to HABs, i.e., via *continuous* dynamic recrystallization (CDRX) during the later stage of deformation. At this stage, the mean grain size was ~0.4 μm (Fig. 4b). In view of the bimodal character of the grain-size distribution, however, this measure was likely not entirely reliable. Alternatively, the volume fraction of ultrafine grains as a function of strain (Fig. 4c) appeared to provide a more reasonable metric. It was found to increase nearly-linearly with strain reaching ~40 pct. in the material with the largest deformation (Fig. 4c).

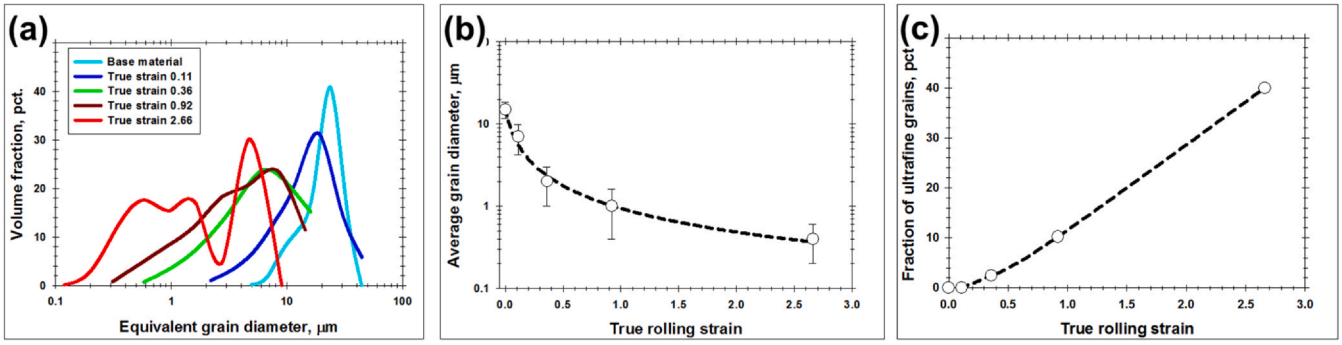

Fig. 4. Effect of rolling strain on: (a) Grain-size distribution, (b) mean grain size, and (c) volume fraction of ultrafine (< 1 mm) grains. In (b), error bars indicate the standard deviation of the measurements.

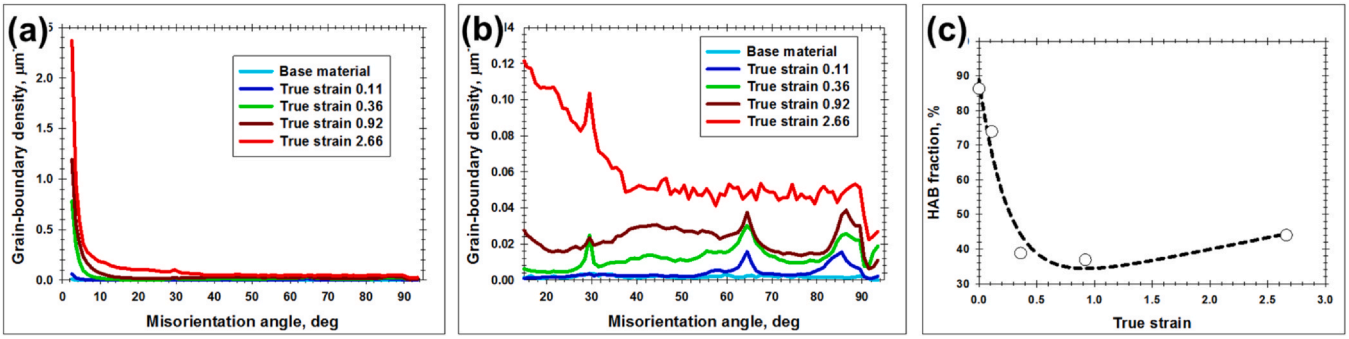

Fig. 5. Effect of rolling strain on: (a) Misorientation-angle distribution for the entire angular range, (b) misorientation-angle distribution for the high-angle range, and (c) the fraction of HABs.

3.4. Grain boundaries

The nature of grain refinement governed by the development of deformation-induced boundaries was further elucidated in plots of misorientation angle (Fig. 5a, b) and misorientation axis (Fig. 6a to e) derived from the EBSD data. Related twin-boundary statistics are summarized in Table 2. In all cases, the misorientation-angle distributions were expressed in terms of grain-boundary density, i.e., boundary length divided by the area of the EBSD map. The theoretical relationship between the various slip systems available in CP Ti and the corresponding misorientation axes of LABs, as derived by Chun et al. [32], are summarized in Table 3 and Fig. 6f.

3.4.1. Behavior for low-to-moderate strains

Inasmuch as the starting program material was supplied in a coarse-grain, fully-recrystallized condition, it was characterized by relatively-low grain-boundary density (Fig. 5a, b), a nearly-random misorientation-axis distribution (Fig. 6a), and a comparatively-high HAB fraction (Fig. 5c). Rolling to a true strain of 0.11 resulted in distinct peaks at 65° and 85° in the misorientation-angle distribution (Fig. 5b) as well as pronounced clustering of misorientation axes near the $<10\bar{1}0>$ and $<2\bar{1}\bar{1}0>$ poles (Fig. 6b). These observations provided evidence of the activation of $\{11\bar{2}2\}$ and $\{10\bar{1}2\}$ twinning (Table 2), or a behavior which is well documented in the literature [4–6,9,10,12–18]. Moreover, an increased fraction of the $35^0 < 10\bar{1}0>$misorientations indicated the operation of $\{11\bar{2}1\}$ twinning (Table 2). In all cases, the observed angular spread around the specific twin-induced misorientation (Figs. 5b and 6b) was likely associated with the gradual transformation of twin boundaries into random ones during the straining process [33].

An increase in strain to 0.36 gave rise to a marked increase in the density of LABs (Fig. 5a). In turn, this resulted in a very large reduction (to ~40 pct.) in the fraction of HABs (Fig. 5c). Equally striking, the rotation axes of LABs (Fig. 6c) were found to align with either the < 0001 > direction or $<6\bar{1}\bar{5}3>$ direction (indicated by the arrow). Per the work of Chun, et al. [32], this provided evidence of the activation of prism < a > and pyramidal < c+a > slip, respectively (Table 3, Fig. 6f). Furthermore, the strengthening of the $65^0 < 10\bar{1}0>$ and $85^o < 2\bar{1}\bar{1}0>$ misorientation peaks (Figs. 5b, 6c) gave evidence that extensive $\{11\bar{2}2\}$ and $\{10\bar{1}2\}$ twinning continued to occur to a strain of 0.36 (Table 2). Another finding of importance was the observation that misorientation axes for 40–50° boundaries tended to cluster in the range of $<30\bar{3}2>$-$<20\bar{2}1>$ (Fig. 6c). This interesting effect was likely associated with secondary $\{10\bar{1}2\} \rightarrow \{11\bar{2}2\}$ twinning, which should produce $41^0 < 5\bar{1}\bar{4}3>$ and $51^0 < 3\bar{1}\bar{2}3>$ misorientations [14].

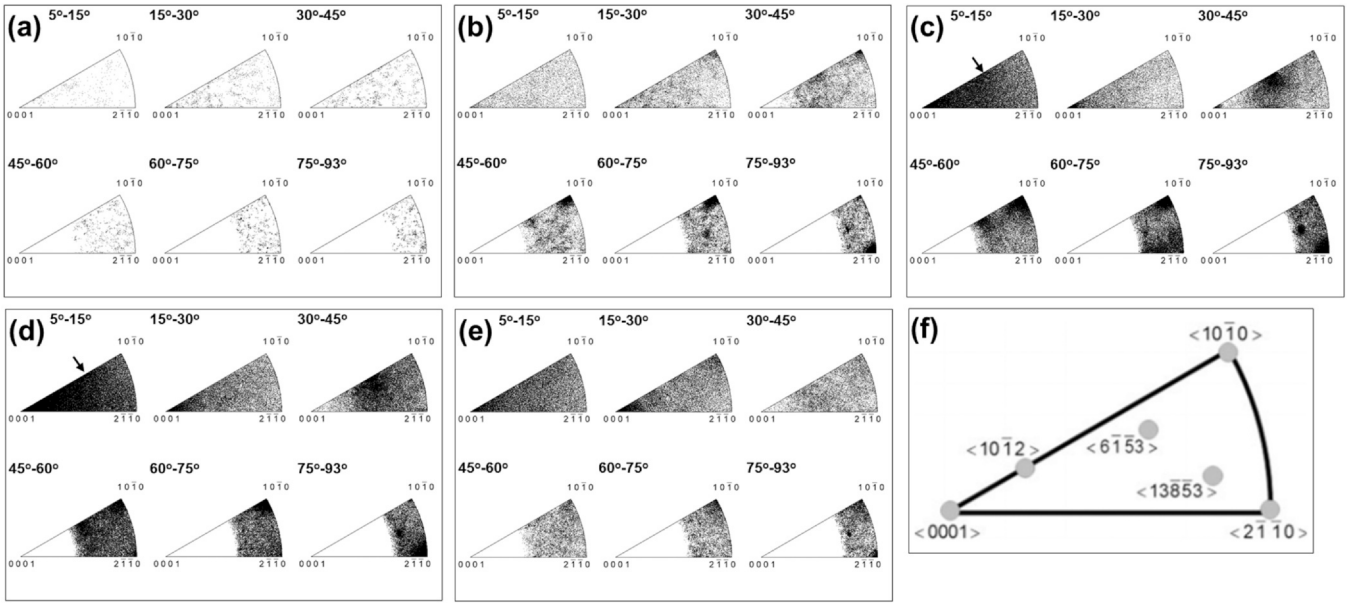

Fig. 6. Effect of rolling strain on misorientation-axis distribution: (a) Base material, and material rolled to a true strain of (b) 0.11, (c) 0.36, (d) 0.92, or (e) 2.66. The standard triangle with the Taylor rotation axes of the slip systems available in alpha titanium is shown in (f) (after Chun et al. [32]). In (c) and (d), arrows indicate the clustering of LAB rotation axes near < 6–1–53 > pole.

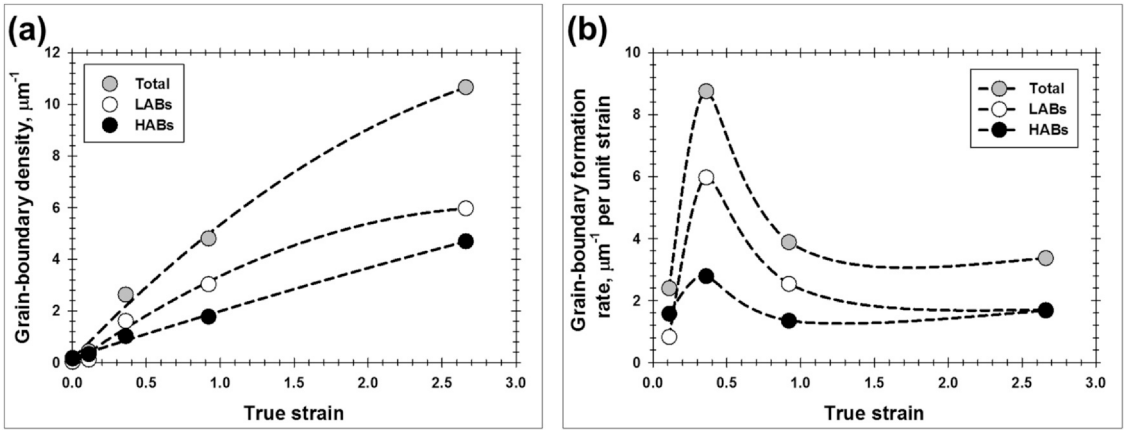

Fig. 7. Effect of rolling strain on (a) Grain-boundary density and (b) the rate of formation of grain-boundaries.

3.4.2. Behavior for high strains

Rolling to true strains of 0.92 and 2.66 promoted a further increase in LAB density (Fig. 5a), thus underscoring the ongoing microstructural refinement. In this context, the significant increase in grain-boundary area in the angular range of ~10–40° (Fig. 5a) as well as the subtle increase of HAB fraction (Fig. 5c) suggested the LAB-to-HAB transformation, i.e., the occurrence of CDRX. On the other hand, the decrease in the twin-boundary fraction to a level comparable to that in the base (starting) material (Table 2) implied essentially an absence of twinning at high strains (Supplementary Fig. S1). Nevertheless, the weak clustering of the rotation axes for 60–75° boundaries near <10$\bar{1}$0> and those of 75–93° boundaries near <2$\bar{1}\bar{1}$0> (Fig. 6e) suggested that some limited amount of twinning may still have occurred even in the high-strain range.

It was also found that the rotation axes of LABs developed at high strains still tended to align with the < 0001 > and <6$\bar{1}\bar{5}$3>directions (Fig. 6d and e). Per Table 3, this observation presumably reflected the dominance of prism- < a > and pyramidal- < c+a > slip in the heavily-rolled material.

3.4.3. Grain-boundary density

The grain-boundary density as a function of strain (Fig. 7a) yielded additional insight into the evolution of grain boundaries during rolling.

The monotonic increase in grain-boundary area was evidence of a progressive refinement in grain size over the entire range of strain used in the present work. The increment of grain-boundary density per unit strain (Fig. 7b) provided a quantitative measure of the *intensity* of this process. The peak rate of the grain-boundary formation process was found at a true strain of ~0.36, likely a result of the combined influence of mechanical twinning and LAB development. The strain for the peak rate of microstructure refinement also coincided approximately with that corresponding with the peak in strain-hardening rate (Fig. 7b vs Fig. 1d).

3.5. Crystallographic texture

The crystallographic aspects of metal flow during rolling CP Ti were further ascertained from alpha phase 0001 and 10$\bar{1}$0 pole figures (Fig. 8) calculated from the EBSD data. The original material had a {*hkil*} < 10$\bar{1}$0> fiber texture (Fig. 8a). Rolling to a true strain of 0.11 resulted in an abrupt crystallographic reorientation toward <0001> //ND (Fig. 8b). This effect is usually attributed to extensive mechanical twinning, as was corroborated by the present microstructure observations (Fig. 3a) and grain-boundary analysis (Table 2).

An increase in strain to 0.36 provided a sharpening of the near- < 0001 > //ND orientation (Fig. 8c), thus signifying a continuation of twinning (Table 2). As shown in Section 3.4.1, however, this strain stage also involved the formation of a substantial number of LABs (Fig. 7b), which, in turn, indicated extensive slip. The dominant (soft) prism- < a > slip mode is known to provide crystallographic rotations

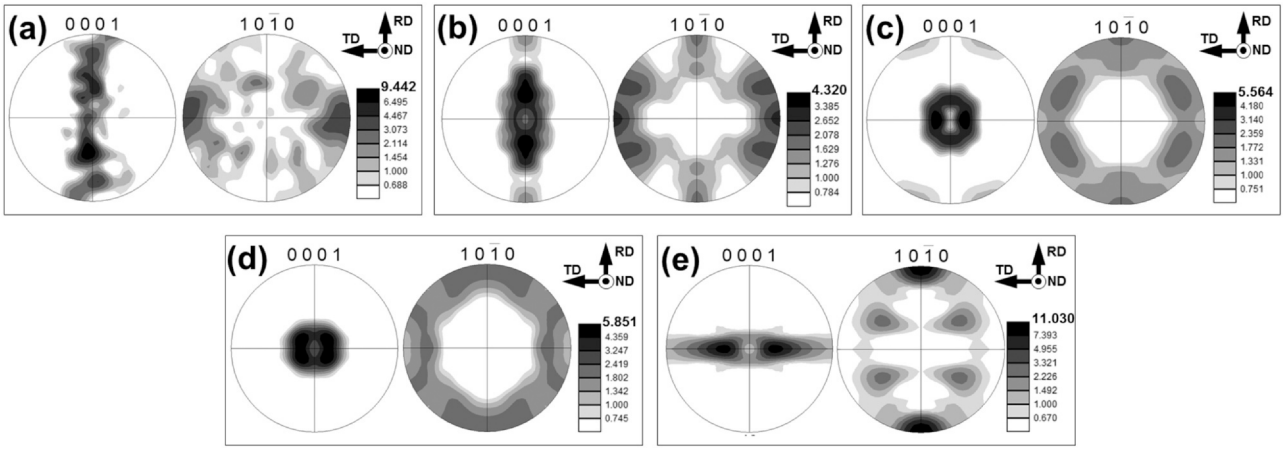

Fig. 8. 0001 and 10–10 pole figures illustrating the evolution of crystallographic texture for: (a) The base material, and material rolled to a true strain of (b) 0.11, (c) 0.36, (d) 0.92, or (e) 2.66.

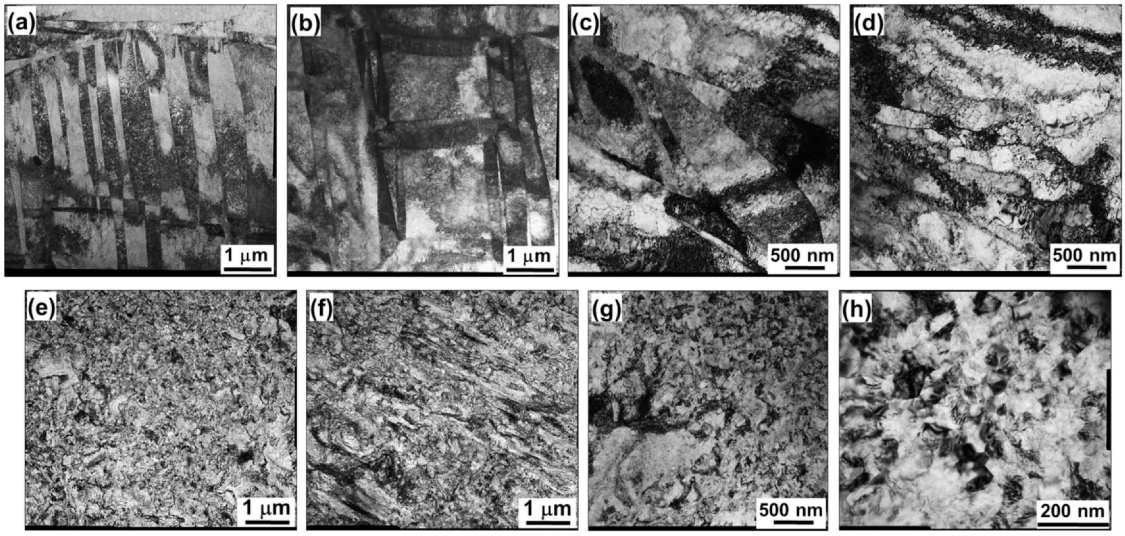

Fig. 9. TEM micrographs showing characteristic microstructural features produced during cold rolling: (a, b) Mechanical twins (true strain of 0.11), (c, d) dislocation boundaries (true strain of 0.36), (e) low-magnification overview of heavily-rolled material (true strain of 1.61), (f) lamellar-type microstructure (true strain of 1.61), (g) coarse-grain remnants (true strain of 2.66), and (h) an ultrafine microstructure (true strain of 2.66).

Table 2
Effect of rolling strain on twin boundary fraction.

Twin mode	Misorientation	Twin-boundary fraction, pct.				
		Base material	True strain of 0.11	True strain of 0.36	True strain of 0.92	True strain of 2.66
$\{11\bar{2}2\}<\bar{1}\,\bar{1}23>$	$65^0<10\bar{1}0>$	0.3	9.0	2.9	1.3	0.3
$\{11\bar{2}1\}<\bar{1}\,\bar{1}26>$	$35^0<10\bar{1}0>$	0.4	0.9	0.1	0.1	0.3
$\{10\bar{1}2\}<\bar{1}011>$	$85^0<2\bar{1}\,\bar{1}0>$	0.4	16.2	3.3	2.0	0.4
$\{10\bar{1}1\}<\bar{1}012>$	$57^0<2\bar{1}\,\bar{1}0>$	0.3	0.1	0.1	0.2	0.1
$\{\bar{1}\,\bar{1}24\}<\bar{2}\bar{2}43>$	$77^0<10\bar{1}0>$	0.3	0.4	0.1	0.0	0.2
$\{11\bar{2}3\}<\bar{1}\,\bar{1}22>$	$87^0<10\bar{1}0>$	0.0	0.2	0.1	0.0	0.2

Note: Instances of an increased fraction of twin boundaries are highlighted in gray.

Table 3
Relationship between slip modes and rotation axes (after Chun et al. [32]).

Slip mode		Rotation axis
Prism	$\{\bar{1}0\bar{1}0\}<2\bar{1}\bar{1}0>$	<0001>
Basal	$(0002)<2\bar{1}\bar{1}0>$	$<10\bar{1}0>$
Pyramidal < a >	$\{\bar{1}0\bar{1}1\}<2\bar{1}\bar{1}0>$	$<10\bar{1}2>$
Pyramidal I < c+a >	$\{\bar{1}0\bar{1}1\}<11\bar{2}3>$	$<13;\bar{8};\bar{5};3>$
Pyramidal II < c+a >	$\{11\bar{2}1\}<11\bar{2}3>$	$<6\bar{1}\bar{5}3>$

around the <0001> direction [32]. Hence, its operation should result in a rotationally-symmetric distribution of intensity in the $10\bar{1}0$ pole figure, as was indeed observed (Fig. 8c). Therefore, the observed texture likely originated from the combined influence of mechanical twinning and prism- < a > slip.

Rolling to a true strain of 0.92 or greater led to the gradual development of a split-basal texture, i.e., {0002} $<10\bar{1}0>$ ± 40° toward the TD (Fig. 8d to e). This texture is typically observed in cold-rolled CP titanium [e.g., 7, 9]. Although its origin is not completely clear, it is usually attributed to the operation of prism- < a > and pyramidal- < c+a > slip systems [7,9].

3.6. TEM observations

TEM observations (Fig. 9) gave insight into microstructure evolution at a very fine scale. At relatively-low strains, as expected, microstructure changes were dominated by pronounced mechanical twinning (Fig. 9a, b) in agreement with observations from optical microscopy (Fig. 2a) and EBSD measurements (Table 2). Broadly similar to the optical and EBSD observations, the twins typically had either a lenticular- or wedge-shaped morphology, and varied in size from several microns to nano-scale dimensions. Within the relatively-coarse primary twins, multiple secondary twinning was often found (Fig. 9a). The activation of several twin variants and/or modes within the same grain resulted in twin intersections which promoted rapid microstructure refinement (Fig. 9b). Equally important, the twins usually contained a relatively-high dislocation density (Fig. 9a and b).

After a true strain of 0.36, extensive dislocation boundaries were observed (Fig. 9c, d), in addition to the mechanical twins. This finding was also in line with EBSD measurements (Figs. 3b and 7b). The dislocation boundaries were often arranged in the form of a lamellar-type microstructure with a mean lamellae intercept width of ~0.5 μm. Surprisingly, no clear dislocation-cell structure was

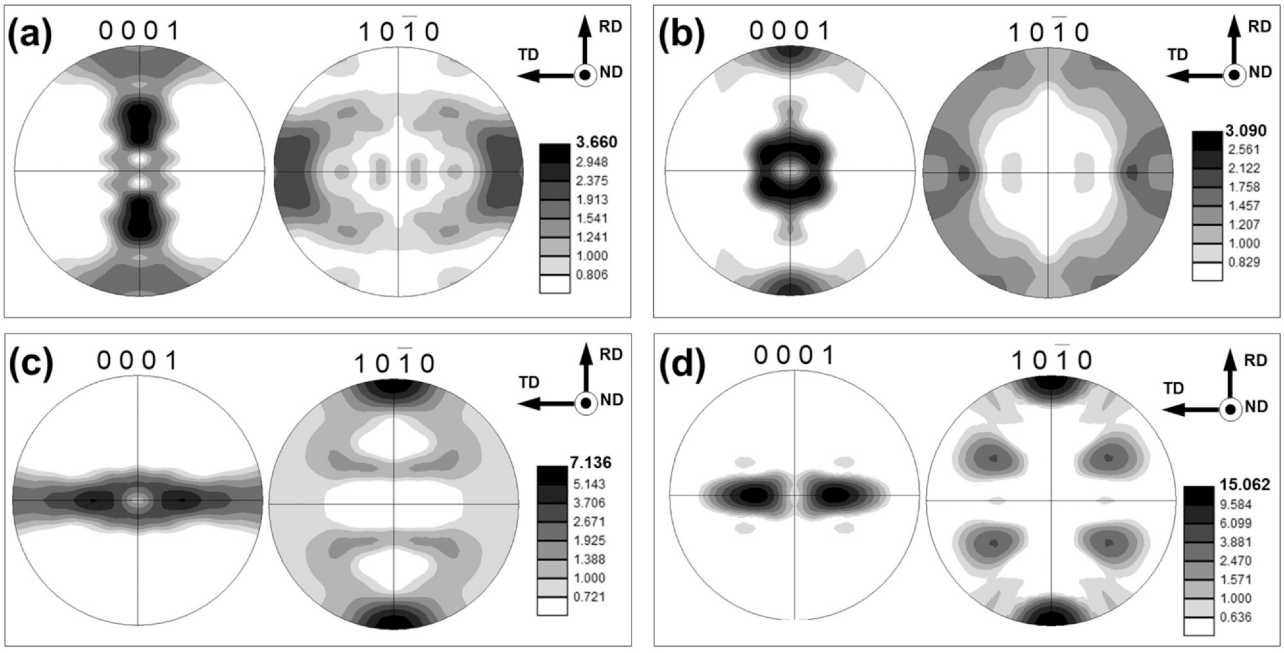

Fig. 10. 0001 and 10–10 pole figures illustrating the effect of rolling strain on crystallographic texture development in ultrafine-grain areas: (a) True strain of 0.36, (b) true strain of 0.92, and (c) true strain of 2.66. In (d), orientations of *remnant* coarse (> 3 μm) grains after a rolling strain of 2.66 are shown.

found, however. Furthermore, the lamellar-type microstructure observed in TEM contrasted with EBSD observations which had a rather irregular distribution as discussed in Section 3.3. This apparent difference implied that a significant portion of the dislocation boundaries revealed by TEM had misorientations *below* the resolution limit of EBSD, i.e., 2 degrees.

With yet further increase in strain to 0.92 and higher, the microstructure became highly-deformed in appearance (Fig. 9e–g). This effect was likely associated with activation of pyramidal-< c+a > slip (as suggested in the previous section) and the concomitant marked increase in dislocation density. Due to the pronounced strain fields developed within the rolled material, the microstructural details became barely recognizable (Fig. 9e). Nevertheless, some evidence of the lamellar-type microstructure could still be observed locally (Fig. 9f). Also, distinct microstructural heterogeneity (or bimodality) was also apparent (Fig. 9g). At very high magnifications, nano-scale grains were also occasionally observed (Fig. 9h). The origin of such features was not clear, however.

4. Discussion

4.1. Crystallographic orientations of ultrafine grains

One of the key processes occurring during rolling of CP Ti to high reductions is the formation of ultrafine grains. The crystallographic orientations of the ultrafine grains extracted from the present EBSD data (Fig. 10a–c) shed more light on this phenomenon. For comparative purposes, the texture of the coarse-grain remnants retained within the heavily-rolled material (Fig. 10d), was also analyzed.

At relatively low strains, the crystallographic orientations of the ultrafine grains were distinctly different from the global texture (Fig. 10a, b vs. Fig. 8c, d). It was likely, therefore, that grain refinement in its early stages was mainly associated with twinning, and particularly secondary twinning. On the other hand, the preferential orientations of the ultrafine grains in the heavily-rolled material were similar to that of the surviving coarse remnant grains (Fig. 10c vs Fig. 10d). This finding likely reflects the CDRX origin of the ultrafine grains, thus being in the line with microstructural observations and analysis of misorientation distributions. Despite this similarity, it is important to emphasize that the 0001 pole figure for the ultrafine-grains was characterized by a noticeable orientation spread toward the TD (Fig. 10c vs Fig. 10d). As mentioned in Section 3.5, prism-< a > slip provides a crystallographic rotation only around < 0001 > [32], and thus this slip mode could not have resulted in such an observation. In light of the suppression of mechanical twinning in the high-strain range, it can thus be deduced that the texture of the ultrafine grains originated from the activation of a *non-prism-* < *a* > slip mode, which was likely pyramidal-< c+a > slip, as suggested in Section 3.4.2.

4.2. Effect of mechanical twinning on strain hardening

The activation of the non-prism-< a > slip modes usually requires relatively-high levels of stress. In this regard, mechanical twinning, which typically occurs during the early stage of deformation of CP Ti, normally results in marked strain hardening [34]. The strengthening effect is usually attributed to grain refinement (i.e., the reduction in average slip length) as well as to the so-called Basinski effect [35]. According to the latter mechanism, glissile dislocations originally in the matrix are immobilized due to twin-induced crystallographic rotations. An additional strengthening factor due to twinning may also be associated with strain-compatibility requirements due to the formation of heterogeneous microstructure.

In the present investigation, the peak strain-hardening rate was observed after a true strain of ~0.1–0.2 (Fig. 1d, e). Such strains coincide with deformation levels corresponding to the highest twinning activity (Table 2, supplementary Fig. S1). Therefore, it can be surmised that the activation of the non-prism-< a > slip modes in the heavily-rolled material was indeed associated with prior mechanical twinning.

4.3. Grain-to-grain interactions

The CRSS for pyramidal-< c+a > slip is of the order of ~3–5 times that for prism < a > slip [36]. On the other hand, the strengthening effect observed in the present work was only approximately twofold (Fig. 1b and c). Such an apparent anomaly can be resolved by noting that the ultrafine grains are typically nucleated at prior grain

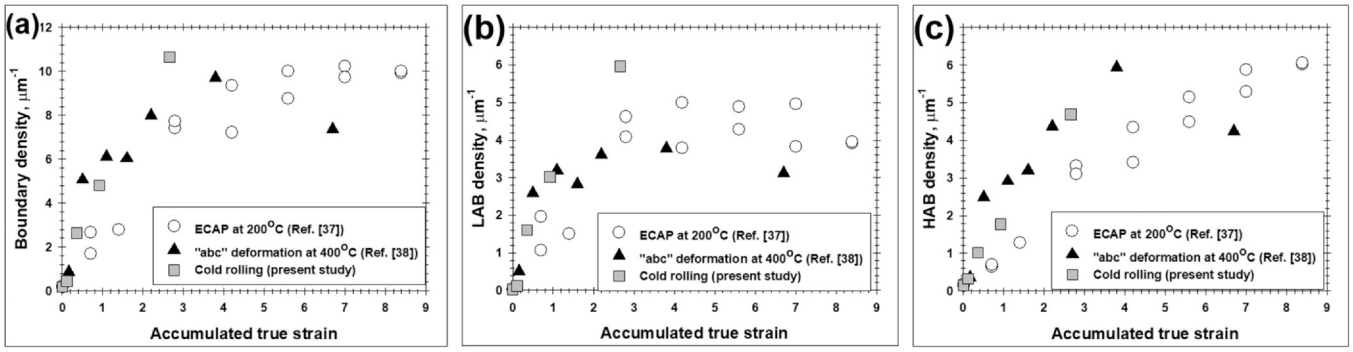

Fig. 11. Evolution of grain-boundary density in CP Ti as function of accumulated true strain for different grain-refinement techniques: (a) Total grain-boundary density, (b) density of LABs, and (c) density of HABs. Note: ECAP denotes the equal-channel angular pressing technique.

boundaries as discussed in Section 3.3. This observation therefore suggests that non-prism- < a > slip was also influenced by grain-to-grain interactions. The interactions can give rise to local stresses higher than the imposed macroscopic stresses which are required for the activation of "hard" slip modes.

4.4. Broad aspects of microstructure refinement during heavy deformation of CP Ti

The relationship between the activation of the non-prism slip mode and the nucleation of ultrafine grains in heavily-strained CP Ti has been reported in several previous investigations [e.g. 37, 38]. Hence, to develop a broad view of the microstructural-refinement process during heavy deformation of this material, the results of the present work were compared with those published in the literature. To this end, the evolution of grain-boundary density as a function of accumulated strain for different grain-refinement techniques was summarized (Fig. 11).

It should be emphasized that the experimental data shown in this figure were obtained under noticeably-different conditions. The key differences included the impurity content in the program material, its initial grain size and crystallographic texture, deformation mode, strain path, and even processing temperature. Nevertheless, the data in Fig. 11 were found to overlap broadly, at least for true strains ≤ 2.7 (i.e., the maximum strain achieved during cold rolling in the present study).[1] This result strongly suggests the operation of a single grain-refinement mechanism which is intrinsic for the heavy deformation of CP Ti.

4.5. Grain-refinement mechanism

From the above results and discussion, it appears that the relatively-high grain-refinement rate typically observed during heavy deformation of CP Ti is attributable to the synergetic effect of mechanical twinning and the activation of non-prism- < a > slip. Twinning alone results in noticeable grain refinement. However, due to the sensitivity of this mechanism to crystallographic orientation as well as its gradual suppression with strain, it is unlikely it can provide the sole basis for the formation of a homogeneous UFG structure. Despite this limitation, considerable material strengthening induced by twinning appears to promote the activation of additional (non-prism- < a >) slip systems, which, in turn, markedly enhances the grain-subdivision process. Due to the relatively-high CRSS for non-prism- < a > slip systems, grain refinement at strains beyond that at which twinning dominates occurs preferentially in local, highly-stressed areas of the microstructure. Typically, such regions lie near the original grain boundaries or within twins and are likely assisted by grain-to-grain (intergranular) interactions. The principal difference in slip activity in the near-grain-boundary regions and within the grain interiors results in diverging crystallographic rotations in these areas and the concomitant development of so-called geometrically-necessary boundaries [39]. The progressive evolution of these boundaries toward high-angle misorientations eventually leads to the preferential formation of ultrafine grains at the grain-boundary regions, thus giving rise to a necklace-type microstructure.

Considering the relatively high dislocation density revealed by TEM (Fig. 9e to h), it is highly unlikely that deformation heating was sufficient to promote significant grain-boundary migration. Hence, it is unlikely that a *discontinuous-type* of recrystallization (i.e., a process involving distinct nucleation and growth stages) contributed to grain refinement. In contrast, a number of experimental observations discussed in Section 3 provided evidence for a dominant role played by a gradual LAB-to-HAB transformation. This process fits the definition of *continuous* dynamic recrystallization. Although the micro-mechanism of the observed LAB-to-HAB transition is not completely clear, it was obviously based on dislocation rearrangement, thus being in essence a recovery-type process, sometimes referred to as "extended recovery" [40]. Moreover, there are several other terms for this phenomenon including "grain fragmentation" [41] and grain subdivision [31]. The distinction between these terms is not clear, however.

5. Summary and conclusions

Using EBSD, the present work has shed light on microstructural changes during the later stags of the cold rolling of CP Ti.

Grain refinement has been found to be governed by a gradual LAB-to-HAB transformation, i.e., a continuous-dynamic-recrystallization (CDRX) mechanism. On the other hand, it was established that the process is closely linked with mechanical twinning occurring during early stages of material flow. Specifically, twinning can give rise to marked work hardening which activates non-prism- < a > slip modes and thus considerably enhances the progressive evolution of dislocation boundaries. As a result, a bulk UFG structure can be produced at modest strains achievable by conventional flat rolling.

Due to the relatively high CRSS of non-prism- < a > slip systems, the activation of such systems typically occurs in local, highly-stressed areas. Typically, this occurs in the proximity of original grain boundaries at which local stresses are heightened due to maintenance of strain compatibility and neighboring-grain

[1] The apparent saturation of microstructure evolution for true strains beyond ~3 observed during ECAP and "abc" deformation is believed to be associated with the change in strain path. Such an effect has been discussed in greater detail elsewhere [38].

interactions. Accordingly, the generation of new, ultrafine grains during cold rolling manifests itself as a necklace-type microstructure.

CRediT authorship contribution statement

S. Mironov: Data curation, Formal analysis, Investigation, Methodology, Software, Validation, Visualization, Writing – original draft. **S. Zherebtsov:** Conceptualization, Investigation, Funding acquisition, Project administration, Supervision, Writing – review & editing. **S.L. Semiatin:** Conceptualization, Writing – review & editing.

Data availability

The raw/processed data required to reproduce these findings cannot be shared at this time as the data also forms part of an ongoing study.

Declaration of Competing Interest

The authors declare that they have no known competing financial interests or personal relationships that could have appeared to influence the work reported in this paper.

Acknowledgments

The authors express their sincere thanks to the staff of the Joint Research Center “Technology and Materials” at Belgorod State National Research University and in particular to Dr. G. Dyakonov for experimental assistance.

Appendix A. Supporting information

Supplementary data associated with this article can be found in the online version at doi:10.1016/j.jallcom.2021.162689.

References

[1] R.Z. Valiev, R.K. Islamgaliev, I.V. Alexandrov, Bulk nanostructured materials from severe plastic deformation, Prog. Mater. Sci. 45 (2000) 103–189, https://doi.org/10.1016/S0079-6425(99)00007-9
[2] R.Z. Valiev, T.G. Langdon, Principles of equal-channel angular pressing as a processing tool for grain refinement, Prog. Mater. Sci. 51 (2006) 881–981, https://doi.org/10.1016/j.pmatsci.2006.02.003
[3] T.G. Langdon, Twenty-five years of ultrafine-grained materials: achieving exceptional properties through grain refinement, Acta Mater. 61 (2013) 7035–7059, https://doi.org/10.1016/j.actamat.2013.08.018
[4] S.V. Zherebtsov, G.S. Dyakonov, A.A. Salem, S.P. Malysheva, G.A. Salishchev, S.L. Semiatin, Evolution of grain and subgrain structure during cold rolling of commercial-purity titanium, Mater. Sci. Eng. A528 (2011) 3474–3479, https://doi.org/10.1016/j.msea.2011.01.039
[5] H.S. Kim, S.J. Yoo, J.W. Ahn, D.H. Kim, W.J. Kim, Ultrafine grained titanium sheets with high strength and high corrosion resistance, Mater. Sci. Eng. A528 (2011) 8479–8485, https://doi.org/10.1016/j.msea.2011.07.074
[6] S.V. Zherebtsov, G.S. Dyakonov, G.A. Salishchev, A.A. Salem, S.L. Semiatin, The influence of grain size on twinning and microstructure refinement during cold rolling of commercial-purity titanium, Metall. Mater. Trans. 47A (2016) 5101–5113, https://doi.org/10.1007/s11661-016-3679-0
[7] N. Bozzolo, N. Dewobroto, H.R. Wenk, F. Wagner, Microstructure and microtexture of highly cold-rolled commercially pure titanium, J. Mater. Sci. 42 (2007) 2405–2416, https://doi.org/10.1007/s10853-006-1302-2
[8] S.V. Zherebtsov, G.S. Dyakonov, A.A. Salem, V.I. Sokolenko, G.A. Salishchev, S.L. Semiatin, Formation of nanostructures in commercial-purity titanium via cryorolling, Acta Mater. 61 (2013) 1167–1178, https://doi.org/10.1016/j.actamat.2012.10.026
[9] Y.B. Chun, S.H. Yu, S.L. Semiatin, S.K. Hwang, Effect of deformation twinning on microstructure and texture evolution during cold rolling of CP-titanium, Mater. Sci. Eng. A398 (2005) 209–219, https://doi.org/10.1016/j.msea.2005.03.019
[10] Y. Zhong, F. Yin, K. Nagai, Role of deformation twin on texture evolution in cold-rolled commercial-purity Ti, J. Mater. Res. 23 (2008) 2954–2966, https://doi.org/10.1557/JMR.2008.0354
[11] S. Nourbakhsh, T.D. O'Brien, Texture formation and transition in cold-rolled titanium, Mater. Sci. Eng. 100 (1988) 109–114, https://doi.org/10.1016/0025-5416(88)90245-5
[12] N. Liu, Y. Wang, W. He, J. Li, A. Chapuis, B. Luan, Q. Liu, Microstructure and textural evolution during cold rolling and annealing of commercially pure titanium sheet, Trans. Nonferrous Met. Soc. China 28 (2018) 1123–1131, https://doi.org/10.1016/S1003-6326(18)64748-X
[13] V.K. Sahu, S. Gupta, N.P. Gurao, Effect of initial texture on the evolution of microstructure and texture during rolling of commercially pure titanium at room and cryogenic temperature, Metall. Mater. Trans. A 51 (2020) 5848–5860, https://doi.org/10.1007/s11661-020-05979-8
[14] N. Bozzolo, L. Chan, A.D. Rollett, Misorientations induced by deformation twinning in titanium, J. Appl. Cryst. 43 (2010) 596–602, https://doi.org/10.1107/S0021889810008228
[15] Y.B. Chun, S.L. Semiatin, S.K. Hwang, Role of deformation twinning in cold rolling and recrystallization of titanium, Mater. Sci. Forum 495–497 (2005) 651–656.
[16] J. Wen, N. Allain, E. Fleury, Hydrogen evolution and its effects on cold rolling behavior in commercial pure titanium, Mater. Charact. 121 (2016) 139–148, https://doi.org/10.1016/j.matchar.2016.10.002
[17] J. Dai, L. Zeng, Z. Li, L. Chai, Z. Zheng, H. Wu, K.L. Murty, N. Guo, Misorientation characteristics and textural changes induced by dense twins in high-purity Ti sheet after small strain rolling, Sci. China Technol. Sci. 62 (2019) 1968–1975, https://doi.org/10.1007/s11431-019-9555-9
[18] X. Li, Y.L. Duan, G.F. Xu, X.Y. Peng, C. Dai, L.G. Zhang, Z. Li, EBSD characterization of twinning in cold-rolled CP-Ti, Mater. Charact. 84 (2013) 41–47, https://doi.org/10.1016/j.matchar.2013.07.008
[19] B. Zhou, R. Yang, B. Wang, L. Deng, Y. Zhang, Twinning behavior of pure titanium during rolling at room and cryogenic temperatures, Mater. Sci. Eng. A 803 (2021) 140458, https://doi.org/10.1016/j.msea.2020.140458
[20] L. Bao, J.-S. Lecomte, C. Schuman, M.-J. Philippe, X. Zhao, C. Esling, Study of plastic deformation in hexagonal metals by interrupted in-situ EBSD measurement, Adv. Eng. Mater. 12 (2010) 1053–1059, https://doi.org/10.1002/adem.201000074
[21] X. Li, J. Li, B. Zhou, M. Yu, M. Sui, Interaction of {11-22} twin variants in hexagonal close-packed titanium, J. Mater. Sci. Tech. 35 (2019) 660–666, https://doi.org/10.1016/j.jmst.2018.09.049
[22] B. Wang, H. Liu, Y. Zhang, B. Zhou, L. Deng, C. Wang, J. Chen, Y. Zhang, Effect of grain size on twinning behavior of pure titanium at room temperature, Mater. Sci. Eng. A 827 (2021) 142060, https://doi.org/10.1016/j.msea.2021.142060
[23] G.S. Dyakonov, S. Mironov, S.V. Zherebtsov, S.P. Malysheva, G.A. Salishchev, A.A. Salem, S.L. Semiatin, Grain-structure development in heavily cold-rolled alpha-titanium, Mater. Sci. Eng. A607 (2014) 145–154, https://doi.org/10.1016/j.msea.2014.03.141
[24] G. Salishchev, S. Mironov, S. Zherebtsov, A. Belyakov, Changes in misorientations of grain boundaries in titanium during deformation, Mater. Charact. 61 (2010) 732–739, https://doi.org/10.1016/j.matchar.2010.04.005
[25] X. Zheng, M. Gong, T. Xiong, H. Ge, L. Yang, Y. Zhou, S. Zheng, J. Wang, X. Ma, Deformation induced FCC lamellae and their interaction in commercial pure Ti, Scr. Mater. 162 (2019) 326–330, https://doi.org/10.1016/j.scriptamat.2018.11.037
[26] F. Bai, Q. Zhu, J. Shen, Z. Lu, L. Zhang, N. Ali, H. Zhou, X. Liu, Study on phase transformation orientation relationship of HCP-FCC during rolling of high purity titanium, Crystals 11 (2021) 1164, https://doi.org/10.3390/cryst11101164
[27] F. Bai, L. Yin, W. Zhao, H. Zhou, M. Song, Y. Liu, X. Liu, Deformational behavior of face-centered cubic (FCC) phase in high-pure titanium, Mater. Sci. Eng. A 800 (2021) 140287, https://doi.org/10.1016/j.msea.2020.140287
[28] Z. Kou, L. Yang, Y. Yang, X. Luo, B. Huang, Hydride or martensite? identification of a new phase in cold-rolled hexagonal close-packed Ti, Mater. Charact. 163 (2020) 110294, https://doi.org/10.1016/j.matchar.2020.110294
[29] Y. Chang, S. Zhang, C.H. Liebscher, D. Dye, D. Ponge, C. Scheu, G. Dehm, D. Raabe, B. Gault, W. Lu, Could face-centered cubic titanium in cold-rolled commercially-pure titanium only be a Ti-hydride? Scr. Mater. 178 (2020) 39–43, https://doi.org/10.1016/j.scriptamat.2019.11.010
[30] F.J. Humphreys, Quantitative metallography by electron backscatter diffraction, J. Microsc. 195 (1999) 170–185, https://doi.org/10.1046/j.1365-2818.1999.00578.x
[31] D.A. Hughes, N. Hansen, High angle boundaries formed by grain subdivision mechanisms, Acta Mater. 45 (1997) 3871–3886, https://doi.org/10.1016/S1359-6454(97)00027-X
[32] Y.B. Chun, M. Battaini, C.H.J. Davies, S.K. Hwang, Distribution characteristics of in-grain misorientation axes in cold-rolled commercially pure titanium and their correlation with active slip modes, Metall. Mater. Trans. 41A (2010) 3473–3487, https://doi.org/10.1007/s11661-010-0410-4
[33] E.V. Nesterova, V.V. Rybin, Mechanical twinning and fragmentation of commercial purity titanium during large plastic deformation, Phys. Met. Metall. 59 (1985) 169–179.
[34] A.A. Salem, S.R. Kalidindi, R.D. Doherty, S.L. Semiatin, Strain hardening due to deformation twinning in α-titanium: Mechanisms, Metall. Mater. Trans. 37A (2006) 259–268, https://doi.org/10.1007/s11661-006-0171-2

[35] Z.S. Basinski, M.S. Szczerba, M. Niewczas, J.D. Embury, S.J. Basinski, The transformation of slip dislocations during twinning of copper-aluminum alloy crystals, La Rev. De. Metall. – CIT/ Sci. Genie Des. Mater. 94 (1997) 1037–1043.
[36] A.A. Salem, S.R. Kalidindi, S.L. Semiatin, Strain hardening due to deformation twinning in α-titanium: constitutive relations and crystal-plasticity modeling, Acta Mater. 53 (2005) 3495–3502, https://doi.org/10.1016/j.actamat.2005.04.014
[37] G.S. Dyakonov, S. Mironov, I.P. Semenova, R.Z. Valiev, S.L. Semiatin, EBSD analysis of grain-refinement mechanisms operating during equal-channel angular pressing of commercial-purity titanium, Acta Mater. 173 (2019) 174–183, https://doi.org/10.1016/j.actamat.2019.05.014
[38] S. Mironov, S. Zherebtsov, S.L. Semiatin, The Unusual Character of Deformation of Commercial-purity Titanium, submitted to Mater. Character.
[39] D. Kuhlmann-Wilsdorf, N. Hansen, Geometrically necessary, incidental and subgrain boundaries, Scr. Met. Mater. 25 (1991) 1557–1562, https://doi.org/10.1016/0956-716X(91)90451-6
[40] O. Engler, M.-Y. Huh, Evolution of the cube texture in high purity aluminum capacitor foils by continuous recrystallization and subsequent grain growth, Mater. Sci. Eng. A 271 (1999) 371–381, https://doi.org/10.1016/S0921-5093(99)00254-3
[41] A.S. Rybtsov, V.V. Rybin, Structural features of plastic deformation at the stage of localized flow, Phys. Met. Metallogr. 44 (1977) 139–149.